frontiers | Frontiers in Materials

TYPE Original Research
PUBLISHED 04 December 2025
DOI 10.3389/fmats.2025.1724720

OPEN ACCESS

EDITED BY
Hao Shi,
Anhui University of Science and Technology, China

REVIEWED BY
Guansheng Han,
Shaoxing University, China
Xiaoxiao Cao,
Kyushu University, Japan

*CORRESPONDENCE
Jun Jiang,
15751096992@163.com

RECEIVED 14 October 2025
REVISED 04 November 2025
ACCEPTED 04 November 2025
PUBLISHED 04 December 2025

CITATION
Jiang J, Sun H, Wang G, Deng X, Li X, Fan W and Liu Z (2025) Improved workability and mechanical properties of cement grouting materials by carbon nanotubes coated with fly ash.
Front. Mater. 12:1724720.
doi: 10.3389/fmats.2025.1724720

Improved workability and mechanical properties of cement grouting materials by carbon nanotubes coated with fly ash

Jun Jiang[1,2]*, Houwei Sun[1,2], Guoyuan Wang[1,2], Xiansong Deng[1,2], Xiaoliang Li[1,2], Wenbo Fan[1,2] and Zhiqiang Liu[1,2]

[1]China Coal No.5 Construction Co. Ltd. The No.3 Engineering Division, Xuzhou, Jiangsu, China, [2]China Coal Construction Group Limited Corporation, Beijing, China

Carbon nanotubes (CNTs) modified cement provides a new way to develop high performance cement grouting materials. However, laboratory-grade CNTs are extremely costly (about 100 times the cost of industrial-grade CNTs) and have poor dispersion stability due to strong van der Waals forces at the nanoscale, which easily cause agglomeration. In addition, the time and energy consumption of CNTs dispersion and the problem of reaggregation further limit their application in engineering. Therefore, a novel dispersion method for CNTs was proposed in this paper. The proposed coating dispersion method not only achieved a good dispersion of CNTs on the surface of fly ash (FA), but also reduced the structural damage of CNTs during the dispersion process. At the same time, a strong covalent bond was formed between CNTs and FA, which effectively alleviated the reagglomeration problem of CNTs. Secondly, the workability and mechanical properties of cement grouting materials reinforced by CNTs coated with FA were studied through laboratory tests. The test results showed that compared with ordinary cement slurry, the fluidity and compressive strength were increased by 3.5%–11.6% and 2.09–32.87% after replacing part of cement with FA coated with CNTs. Finally, the mechanism of CNTs' influence on the microstructure of the grouting material was studied through the microcharacterization test. The results showed that CNTs coated on the FA surface produced nucleation effect and played a bridging role, promoted hydration reaction and improved the cement-FA interface transition zone (ITZ). In addition, CNTs coating FA effectively improved the energy absorption effect of the cement matrix, resulting in changes in the micro-roughness of the fracture surface of the sample.

KEYWORDS

carbon nanotubes, cement grouting materials, nanomodification, engineering properties, preparation optimization

1 Introduction

Due to its ability to strengthen structures and prevent leakage, grouting reinforcement techniques have been used in a wide range of engineering applications, including transportation facilities, tunneling, mining operations, slope stabilization, new energy development, and nuclear waste management (Güllü et al., 2019; Han et al., 2020;

Jing et al., 2020; Liu et al., 2020; Hamid Abed et al., 2022; Shi et al., 2022; Wu et al., 2025a). With the continuous development of grouting technology, the types and quantities of grouting materials are increasing, and the main classifications include cement, water glass, chemical, and composite. Chemical grouting materials generally have high cost, high technical requirements and great impact on the environment. All these problems hinder its wide application in engineering. Cement grouting materials are widely used in grouting projects due to their wide source of raw materials, simple preparation, low cost and excellent consolidation performance.

Given the project's expanding scale and intricate engineering settings, elevated demands are imposed on attributes like strength, fluidity, injectability, impermeability, stability, and durability of cement grouting materials. To address this, numerous researchers have explored enhancing specific properties of the slurry by incorporating clay, lime powder, bentonite, silica fume, FA, blast furnace slag, and other mineral particles into the grouting material. These methods not only improve the specific properties of the cement paste to address different engineering problems, but also utilize industrial waste, reducing costs and reducing environmental stress. For example, adding composite clay to cement grouting material can improve its impermeability. (Garzón et al., 2015; Shi et al., 2023; Wu et al., 2025b); Incorporating lime powder markedly enhances the flow characteristics of cement grouting materials (Svermova et al., 2003). Mixing bentonite clay achieves the objective of enhancing the slurry's stability (Abdel Rahman et al., 2013; Shi et al., 2025). The strength of the grouting material is increased by introducing silica fume into the cement slurry (Langan et al., 2002; Song et al., 2010). And incorporating FA enhanced both the flow properties and long-term strength (Ferreiro et al., 2017; Rakngan et al., 2018). In addition to the above materials, some scholars have also investigated the use of polypropylene fibers (Feng et al., 2021), carbon fibers (Chuang et al., 2017), steel fibers (Nguyen et al., 2010) and other materials to enhance the physical properties of cement grouting materials to improve its application in engineering.

Although these additives can improve the performance of the gel grouting material, they also introduce new problems. (Liu et al., 2021). FA and blast furnace slag have complex effects on slurry performance, including slow strength growth, seasonal limitations, increased need for air-entraining agents, and higher proportions of FA that can lead to salt scaling (Wang et al., 2021). Other additives such as fiber materials (Pedroso and Flores-Colen, 2020; Wu et al., 2025c) and nanoparticles (Kong et al., 2014; Zhang et al., 2024) can also optimize the pore structure of cementitious materials and improve the consolidation strength, but they are difficult to be widely used in practical engineering due to the problems of flow performance and cost. Although the above additives can optimize the performance of cement-based materials, the compatibility between nanoscale CNTs and other admixtures remains a key unresolved issue in engineering applications—their interaction may produce synergistic effects or mutual inhibition, directly affecting the stability of modification effects. From the perspective of synergistic effects, polycarboxylate superplasticizers (PCE) can assist the dispersion of CNTs in cement slurry through electrostatic repulsion and steric hindrance effects: Collins et al. (2012) found that when the PCE dosage is 0.2%–0.3% of the cementitious material, the van der Waals force between CNTs can be significantly weakened, reducing the particle size of CNT aggregates from 500 nm to less than 100 nm while maintaining slurry fluidity; Gao (2019) further confirmed that the synergistic effect of PCE and CNTs can promote the early hydration of cement, increasing the 28-day compressive strength by an additional 8%–12%. In addition, the combination of CNTs and silica fume can form a "nucleation-filling" synergistic mechanism: Cheng et al. (2023) pointed out that the micro-aggregate filling effect of silica fume can reduce the pores of the cement matrix, while the nucleation sites provided by CNTs can guide the growth of hydration products in the pores, and the two together increase the compactness of the cement-FA interface transition zone (ITZ) by more than 20%.

However, some admixtures have inhibitory effects with CNTs: Kang et al. (2015) found that traditional naphthalene-based superplasticizers and CNTs have competitive adsorption, and naphthalene-based molecules tend to be preferentially adsorbed on the surface of CNTs, making it impossible for CNTs to combine effectively with cement particles, and instead reducing the slurry fluidity by 15%–20%; in addition, when high-content polypropylene fibers (>0.3%) are mixed with CNTs, the fiber surface is easy to entangle CNTs to form secondary agglomeration, leading to stress concentration points inside the matrix, and reducing the flexural strength improvement from 18% to less than 5%. The above compatibility issues indicate that simply introducing CNTs or a single admixture is difficult to balance material performance and engineering applicability. Therefore, it is urgent to develop a new dispersion technology that can coordinate the interaction between CNTs and admixtures, which is also an important starting point for proposing the "CNT-coated fly ash" method in this paper. It is clear that, although there is considerable research on the improvement of cementitious composites, existing technologies tend to negatively affect the fluidity, stability, and transport diffusion of the slurries, which makes it a challenge to enhance the strength, impermeability, durability, and processability of cementitious slurries while controlling the cost at the same time. Therefore, there is an urgent need to develop better cementitious materials to meet these challenges.

In recent years, with the rapid development of the field of nanomaterials, it is possible to realize the high performance development of traditional cement materials by combining nano modification technology (Del Carmen Camacho et al., 2014). Among them, research on CNTs has made significant progress in the past few years. CNTs can provide more nucleation sites and promote hydration of cement. In addition, the bridging effect of carbon nanotubes can also reduce the gap between the hydration products, thereby reducing the porosity. Numerous studies have proved that a large number of studies have shown that the incorporation of a very small amount of CNTs not only does not adversely affect the fluidity, workability and stability of the slurry of cementitious materials, but also can be effective in optimizing the pore structure of the cementitious materials, enhancing their mechanical properties, and durability (Parveen et al., 2015; Liew et al., 2016; Chen and Akono, 2020; Wang et al., 2022; Wu et al., 2025a). In addition, when partial FA is used instead of cement, the activity of fly ash is low and the reaction rate is slow, which will seriously affect the properties of the material. CNTs can provide more nucleation sites for fly ash and cement, and the charge effect can also regulate metal cations

to form denser hydration products. However, there are still gaps in current long-term durability research: in terms of impermeability, Wu et al. (2022) found that CNTs can reduce the chloride diffusion coefficient by 25%–30%, but only monitored up to 28d, without involving the impact of long-term dispersion on seepage channels; in terms of frost resistance, Zhang et al. (2024) confirmed that CNTs can reduce freeze-thaw cracks, but did not consider the risk of CNT secondary agglomeration under long-term freeze-thaw; in terms of corrosion resistance, Cheng et al. (2023) pointed out that CNTs can block SO_4^{2-} transmission, but did not analyze the long-term mechanism combined with ITZ micro-evolution. These gaps limit their application in high-demand projects and highlight the value of this study's "CNT coating method" in improving long-term stability.

However, the nanoscale and extremely high specific surface area of carbon nanotubes can lead to strong van der Waals gravity between them, which may cause them to form aggregates. It has been shown that agglomerated CNTs not only weaken the enhancement of the microstructure of the cementitious paste but also cause defects, weak zones, and stress concentration in the cement matrix (Kim et al., 2019). In order to improve the dispersibility of carbon nanotubes, researchers proposed that carbon nanotubes should be well dispersed and mixed with cement in the form of an aqueous suspension, and developed ultrasonic dispersion, addition of surfactants, functionalization, and hybridization to prepare highly dispersible carbon nanotube suspensions. For the hybrid of a variety of carbon nanomaterials, even without the use of admixtures, a stable dispersion can be formed in water, and the enhancement of a variety of carbon nanomaterials can be synergically played, but an ultrasonic generator is still needed to remove its initial agglomeration.

In this study, industrial-grade CNTs were used as reinforcing materials and 20wt% of cement was replaced with FA. Both CNTs and FA used are industrial by-products and therefore have a good cost effect. By modifying CNTs and FA, CNTs were coated on the surface of FA particles, and the coating effect of CNTs on the surface of FA particles was verified by microscopic characterization experiments. The rheological properties of composite cement grouting materials were evaluated by micro-slump test and digital rotary viscometer. Then mechanical experiments were carried out to verify the strengthening effect of CNTs on the grouting material. After the mechanical test, high-precision 3D laser scanner, backscatter electron imaging and scanning electron microscope were used to obtain the micromorphology of the fracture surface of the sample. The microscopic data obtained were analyzed with matlab program to further reveal the strengthening effect of CNTs on ITZ grouting material and the influence on the roughness of the fracture surface. The experimental results finally show that this method is expected to promote the application of CNTs in practical grouting projects in the future.

2 Materials and methods

2.1 Materials

The industrial-grade multi-walled carbon nanotubes (MWCNTs) used in this study are by-products of the methane cracking to hydrogen process, and their specific production process refers to the industrial preparation technology of Chen et al. (2022): high-purity methane (CH_4, purity >99.9%) was used as the raw material, and high-temperature cracking was carried out in a continuous fixed-bed reactor under the action of a supported nickel-based catalyst (Ni/Al_2O_3, Ni mass fraction 5%–8%) (reaction temperature 850 °C–900 °C, reaction pressure 0.1–0.2 MPa); methane molecules decomposed into carbon atoms and hydrogen (H_2) on the catalyst surface, carbon atoms formed multi-walled carbon nanotubes through surface diffusion and precipitation, hydrogen was collected as the main product, and MWCNTs were captured from the reaction tail gas by cyclone separation and filtration, and finally obtained after low-temperature drying (60 °C, 2 h) to remove residual adsorbed gas.

The impurity composition and content of MWCNTs prepared by this process were determined by X-ray fluorescence spectroscopy (XRF) and thermogravimetric analysis (TGA), including: residual catalyst metals (Ni, Al, total mass fraction <1.2%), amorphous carbon (mass fraction 1.5%–2.0%), trace ash (mainly SiO_2, mass fraction <0.3%) and incompletely desorbed methane (volume fraction <0.1%). Previous studies have shown that this impurity content does not significantly affect cement hydration and the reinforcement effect of CNTs (Chen et al., 2022), and its cost is only 1% of laboratory-grade MWCNTs, which has potential for engineering application. The physical characteristics of the CNTs used in the experiment and the composition of cement and fly ash are presented in Tables 1, 2, respectively.

2.2 Sample preparation

The process of coating CNTs onto the surface of FA has been deeply studied by scholars (Mortazavi et al., 2019; Nguyen et al., 2021), and we have made some modifications to it in this study, and the preparation process and the basic principle are schematically shown in Figure 1.

Amino functionalization of FA consists of soaking FA in hydrochloric acid solution for 2 h, followed by multiple rinses with large amounts of deionized water. The FA with impurities removed was then dried in an oven at 110 °C for 5 h. After cooling to room temperature, 100 g of FA was weighed and added to 100 mL of 5% 3-aminopropyltriethoxysilane solution and stirred magnetically at 70 °C for 1 h to fully react FA with the coupling agent and achieve amino-functionalization of FA. Next, the FA that had completed amino-functionalization was washed several times using deionized water. Finally, the amino-functionalized FA was collected after drying in an oven at 110 °C for 5 h.

Acidification of carbon nanotubes: First, a small amount of carbon nanotubes was added to the mixed acid solution and then stirred continuously for 1 h with a magnetic stirrer. The solution was diluted in distilled water and filtered using a PTFE membrane with

TABLE 1 The physical characteristics of applied CNTs.

Purity	Pipe diameter	Pipe length	Specific surface area
~97%	7–15 nm	5–10 μm	250–500 m^2/g

10.3389/fmats.2025.1724720

TABLE 2 Composition of cement and fly ash (FA) (%).

	CaO	SiO_2	Al_2O_3	Fe_2O_3	SO_3	MgO	TiO_2	Others	Loss
Cement	65.01	20.69	5.71	4.18	2.52	0.61	0.31	0.32	3.26
FA	2.27	53.36	29.09	3.87	-	0.81	-	6.4	2.48

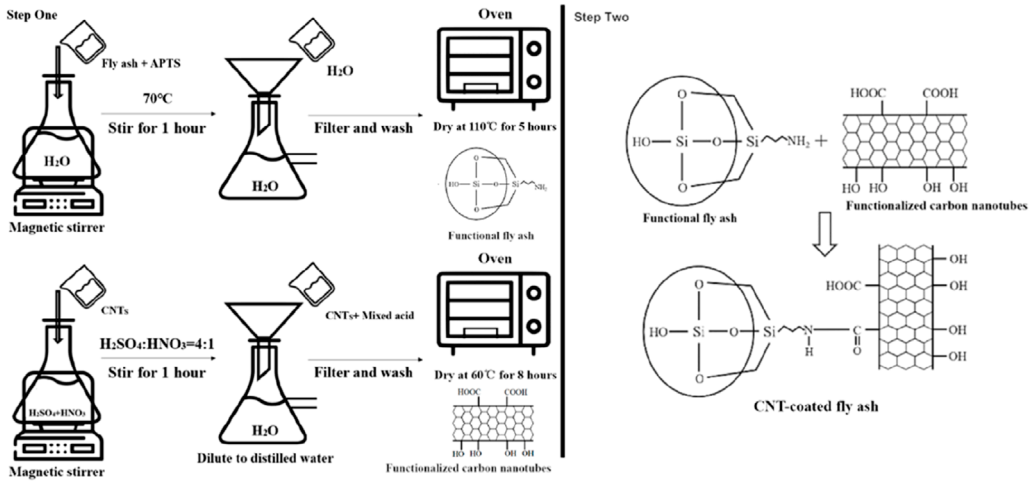

FIGURE 1
Schematic illustration of the fabrication process of CNT coated FA.

a pore size of 0.45 μm. The obtained sample was washed and filtered using distilled water until neutral. Finally, the acid-functionalized carbon nanotubes were collected after drying in an oven at 60 °C for 8 h. CNTs have high thermal stability and can maintain their structure and mechanical properties at higher temperatures, so drying them in an oven will not affect their properties.

The amidation reaction between amino and carboxyl groups can realize the coating of CNTs on the surface of FA. Amino-functionalized FA and acid-functionalized CNT were mixed in an aqueous solution and stirred in a magnetic stirrer for 2 h to ensure that the amino-functionalized, acid-functionalized CNT reacts sufficiently with the FA. Next, it was dried in an oven at 110 °C for 5 h. The carbon nanotube-coated FA was collected after drying and cooling to room temperature in an oven. The activity of fly ash is low, and too high proportion will significantly reduce the mechanical properties of grouting materials due to inadequate reaction. Therefore, 20wt% fly ash is finally selected to replace part of the cement. The dosages of CNTs and polycarboxylic acid water reducing agent were selected to be 0.032% and 0.256% of the cementitious material, respectively. This is because, at this particular ratio, CNTs exhibit excellent enhancement and have been shown to have a cost effect (Gao, 2019).

In order to more accurately assess the feasibility of this chemical coating process and analyze the enhancement effect of CNTs on composite cementitious materials under this dispersion method. In this study, four groups were set up, control group 1 was pure cement slurry (Ref); control group 2 was cement-FA slurry (CFAS); control group 3 was ultrasonic CNTs-reinforced cementitious slurry (UCNTCS); and the experimental group was coated CNTs-reinforced cementitious slurry (CCNTCS). For the UCNTCS group, the carbon nanosuspension was first prepared: the weighed polycarboxylic acid water reducer and CNTs were dissolved in distilled water and stirred in a magnetic mixer for 10 min, followed by ultrasonication of the mixed solution to obtain the carbon nanotube suspension. In addition to affecting the dispersion of CNTs, polycarboxylic acid superplasticizers also greatly affected the fluidity of grouting materials. Therefore, Ref group and CFAS group used the same amount of superplasticizers. The ultrasonic treatment equipment was selected as VCX500 ultrasonic instrument and set to pulse mode with a single pulse time period of 6 s (3 s pause after every 3 s of energy release). The sonication time and power were 10 min and 150 W, respectively, and the suspension was placed in an ice-water bath to prevent overheating during the sonication process; for the CCNTCS group, the carbon nanotube-coated FA suspension was first prepared: the weighed polycarboxylic acid water reducing agent and the prepared carbon nanotube-coated FA were dissolved in distilled water and stirred in a magnetic mixer for 10 min to obtain the carbon nanotube-coated FA suspension.

Following this, the mixture of cement, FA, and suspension was thoroughly blended and then poured into a 50 mm diameter, 100 mm high mold. Vibrate for 1 min to remove air from the slurry. Subsequently, the mold's top was sealed using PTFE film before being placed in a curing box at 20 °C ± 1 °C with a relative humidity exceeding 95% for 24 h. After the initial curing period, the mold was taken out, and the samples were left to continue curing in the same

conditions for an additional 27 days. Once the curing process was completed, the specimens were cut, sanded, and prepared for testing mechanical properties.

2.3 Characterization method

2.3.1 Microscopic characterization of the coating effect of CNTs

First, scanning electron microscope (SEM) was used to characterize the morphology of FA particles and FA particles coated with CNTs. Then, the functional groups and bonding modes in the common FA and the FA coated with CNTs were determined by X-ray photoelectron spectroscopy, Raman spectroscopy and infrared spectroscopy.

2.3.2 Workability tests

Proper workability is a prerequisite for cement composite materials to maintain density and homogeneity, and is crucial for the physical and mechanical properties and durability of cement grouting materials (Makul, 2021). In this study, slurry workability was determined by micro-slump test and digital rotational viscometer test. The measurement procedure of the micro slump test is as follows:

First, the cleaned miniature slump cone was placed on a horizontal Plexiglas plate. Second, a fresh composite cementitious slurry was poured into the miniature slump cone. Next, the side walls of the cone were gently tapped and excess air bubbles at the top were obliterated. Subsequently, the miniature slump cone is lifted vertically and quickly, and the slurry flows through the plexiglass plate under the action of gravity and hydrostatic pressure. When the internal friction and hydrostatic pressure within the slurry reach equilibrium, the flow stops. Ultimately, the horizontal measurement was taken for the outer edge diameter of the circular region created by the slurry, vertical and diagonal directions (up to 45°) and averaged as a result of the miniature slump test.

A rotational viscometer was employed to assess the rheological characteristics of cement grouting materials. Prior to the start of the test, a well-mixed slurry was filled into a measuring cup at room temperature (20 °C), the height of the viscometer was adjusted until the first notch of the rotor was submerged by the slurry, and the rotational viscometer was subsequently activated to measure the shear stress of the slurry. The cement slurry was poured into the measuring cylinder and left to stand for 240s. The shear rate was set to 0.01 s^{-1}. During the test, each test interface lasted for 30s, with a time interval of 1s between each adjacent test point.

2.3.3 Mechanical testing

In this research, the mechanical properties of carbon nanocomposite cementitious grouting materials were evaluated using an MTS815 electronic servo-hydraulic testing machine. The loading rate is set to the international recommended value of 0.1 mm/min. Test specimens for uniaxial compression comprised cylinders measuring 50 mm in diameter and 100 mm in height. Post-testing, micro-morphological attributes of specimen fracture surfaces were captured using a high-precision three-dimensional laser scanner, After mechanical testing, a high-precision 3D laser scanner (Model: Keyence VR3000, Keyence Corporation, Japan), backscattered electron microscope (BSE), and scanning electron microscope (SEM) were used to obtain the micromorphology of the fracture surface of the specimen. Among them, the core measurement accuracy parameters of the 3D laser scanner are as follows: point cloud resolution 0.5 μm, scanning range 50 × 50 mm - 100 × 100 mm, Z-axis measurement accuracy ±2 μm, plane measurement accuracy ±1 μm, scanning speed 300,000 points/second; this instrument realizes non-contact scanning through blue laser (wavelength 405 nm), which can effectively avoid damage to the microstructures of the fracture surface and ensure that the obtained 3D point cloud data accurately reflect the undulation characteristics of the fracture surface. The data obtained from the micro-experiment were processed using Matlab software tool, which assisted researchers in mathematical statistics, induction, and geometric processing of the data to reveal the mechanism of CNTs' influence on the fracture characteristics of composite cement grouting materials, a backscattered electron microscope, and a scanning electron microscope. Matlab software tool is used to process the data obtained from the micro-experiment. matlab software can assist researchers in mathematical statistics, induction, and geometric processing of the data to reveal the mechanism of CNTs' influence on the fracture characteristics of composite cement grouting materials.

3 Results and discussion

3.1 Microscopic characterization of the coating effect of CNTs

In order to study the coating effect of carbon nanotubes on FA, the FA suspension was prepared first, and then the microscopic morphology of fly ash was characterized by SEM. The microscopic morphology of the common FA and CNTs-coated FA particles are shown in Figures 2a,b. Vegetable FA particles are spherical, with a diameter of about 13.8–17.1 μm, and have a smooth surface. Previous studies have shown that this unique geometry and surface properties allow FA to create a ball-bearing effect and a dispersion effect (Payá et al., 1996) in cement mixtures to reduce the friction between cement (or cement and aggregate) and to fill the gaps between cement particles or flocculated structures, thus releasing water from these structures to improve the slurry's workability.

A large number of CNTs encapsulated on a single FA particle is illustrated in Figure 2a. It can be observed that the FA surface is densely and uniformly distributed with CNTs of several micrometers in length, and also a significant portion of CNTs are embedded within the FA at one end and open to the outside at the other end. Previous studies have shown that the slower hydration rate of FA compared to cement results in the formation of a highly porous interfacial transition zone between the FA particles and the cement matrix (Diamond, 1996). It is speculated that CNTs coated on the surface of FA particles will help to improve the interface characteristics of FA and cement matrix and the mechanical properties of composite cement grouting materials, because CNTs can exert nucleation effect, promote the hydration reaction between FA and cement, form a denser cement/FA interface, and thus

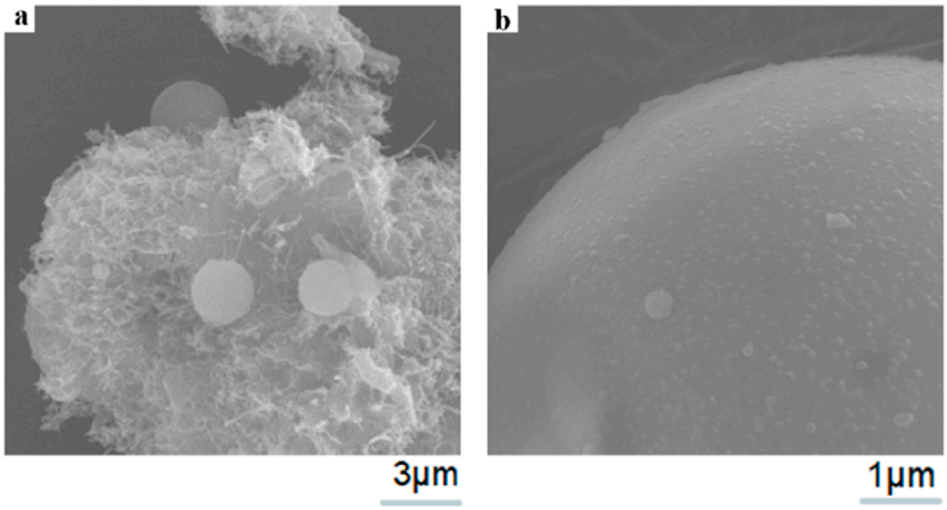

FIGURE 2
SEM characterisations of **(a)** the CNT-coated FA particles plain FA and **(b)** the plain FA.

improve the mechanical properties of hardened composite cement grouting materials.

In previous studies, microscopic characterization methods such as X-ray photoelectron spectroscopy, Raman spectroscopy and infrared spectroscopy were used to determine the functional groups and bonding modes contained in the common FA and carbon nanotube-coated FA (Cheng et al., 2023). The results showed that only oxygen (O1S) peak was observed in the energy spectrum of ordinary FA, while carbon (C1S) and nitrogen (N1S) additional characteristic peaks could be observed in the energy spectrum of FA coated with CNTs. C-c, C-O-C and C=O peaks were found at the position of carbon peaks, which was consistent with that of acid-functionalized CNTs (Yao et al., 2019).The characterization results showed that CNTs were attached to the surface of FA particles. The nitrogen peak, on the other hand, corresponds to the amino group introduced during the reaction of FA with 3-aminopropyl triethoxysilane. The oxygen peak intensity became larger indicating that the oxygen content on the FA surface increased after encapsulating carbon nanotubes, which is mainly due to the oxygen-containing groups carried by the acid-functionalized CNTs and 3-aminopropyltriethoxysilane itself as well as the oxidative reaction during the encapsulation process.

The Raman spectra of both common FA and carbon nanotube-coated FA show the presence of D and G peaks. The D peaks are mainly from C-C bonds and C=C double bonds, and their intensities mainly reflect the structure and defects of the samples (Ferrari and Basko, 2013). The G peak primarily arises from the interatomic vibration among sp^2 carbon atoms, with its intensity indicating the structural integrity of the carbon material lattice (Kaniyoor and Sundara, 2012). The existence of D and G peaks in the common FA is due to the impurity carbon mixed between the FA. The increase in the intensity of the D peak after the FA is coated with CNTs is mainly due to the presence of defects in the acid-functionalized carbon nanotubes encapsulated (Potgieter-Vermaak et al., 2006), this implies that the coating treatment has not impacted the internal quality of the carbon nanotubes.

Characteristic peaks are present in the infrared spectra of both the common FA and FA coated with CNTs (Mortazavi et al., 2019), which correspond to Si-O-Si bonds, Si-OH groups and C=O groups, respectively. When the CNTs were encapsulated on the FA surface, their spectrograms showed a prominent external peak, which indicated the pull-up of the C=O group in the sec-amides (Wang, 2015) and demonstrated the existence of strong covalent bonds between the CNTs and FA.

Even if well-dispersed CNTs suspensions were obtained by traditional dispersion methods, CNTs would inevitably enrich and reagglomerate after the suspensions were added to the cement grout. CNTs coated on the surface of FA particles were not only uniformly distributed in the grout by the help of FA particles during agitation, but also firmly connected to FA by the power of covalent bonds, greatly reducing the free CNTs. Thus, the occurrence of reaggregation is reduced.

3.2 Workability tests

The results of the micro-slump test are shown in Figure 3a. The average slump diameter of ordinary cement slurry (Ref) was about 144.3 mm, and when 20% of the cement in the cementitious grouting material was replaced with an equal amount of FA, the slump diameter of the FA composite cementitious slurry (CFAS) increased to about 155.7 mm, which is an increase of 7.9% compared to the ordinary cement slurry. This is mainly due to its smooth surface, spherical structure and small particle size, FA can produce ball bearing effect and dispersion effect in cement mixtures to reduce the friction between cements and fill the gaps between cement particles or flocculated structures, releasing water from these structures, thus significantly improving the slurry's compatibility.

After the addition of ultrasound-treated CNTs in CFAS group, slump diameter decreased from 155.7 mm to 153.4 mm, with

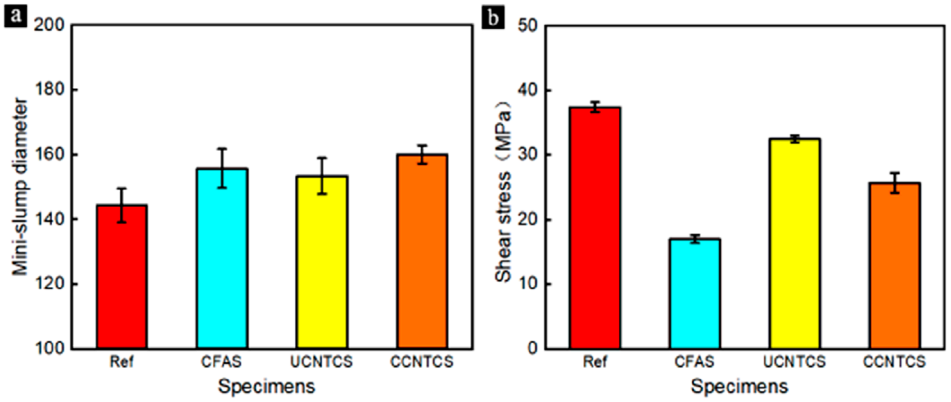

FIGURE 3
(a) micro-slump test results and **(b)** shear stresses of four groups of grouted materials.

a reduction of about 1.5%. Because CNTs (especially CNTs agglomerates) have a large specific surface area (producing high surface energy), it is easy to adsorb and capture free water in the cement slurry, and the reduction of free water increases the friction between cement particles, resulting in reduced workability. It has been reported that the addition of only 0.05%–0.1% CNTs (mass ratio to cement) to cement slurry without the addition of admixtures and auxiliary cementitious particles resulted in a 16.7%–32.8% decrease in the workability of fresh slurry (Collins et al., 2012; Kang et al., 2015). It should be noted that moderate amounts of surfactant and FA were added to the cement slurry in this study, significantly attenuating the negative effects that CNTs have on fresh slurry compatibility.

Compared with traditional ultrasonic CNTs, the workability of CNTs composite cement-base grouting materials (CCNTCS) prepared by coating the surface of CNTs was significantly improved. It can be found that the slump diameter of the CCNTCS group is about 161.1mm, which increases by 3.5%–11.6% compared with the other three groups. On the one hand, the side chains of 3-aminopropyltriethoxysilane lubricate the cement particles and produce a spatial site-blocking effect, hindering the flocculation of the cement (Li, 2018). On the other hand, the strong covalent bonds between CNTs and FA hindered the separation of CNTs from FA particles during the mixing process. As a result, there are fewer free CNTs in the cement matrix, which helps to reduce the number of CNTs aggregates and thus reduce the capture of free water. The cement hydration has more free water available, thus improving the flow of the slurry.

The rheological property test results for the four sets of cement grouting materials are displayed in Figure 3b. Incorporating FA particles enhances the slurry's fluidity but notably decreases its shear stress, reducing the final peak shear stress from 37.8 MPa to 16.2 MPa, marking a 57% decrease compared to standard slurries. This result is in line with the expectation that the ball effect and pore filling effect of fly ash will not only improve the workability of the slurry, but also weaken the peak shear stress of the slurry. The peak shear stress of CNTs composite cement-based slurry rose sharply, reaching 32.5 Mpa and 25.7 Mpa, respectively. Comparing the test results of four groups of cement samples, it can be found that the conclusions of rheological test and slump test are basically the same. In general, CNTs coating FA has a positive effect on the workability of the composite cement grouting material.

3.3 Mechanical property

Figure 4 show the average values of 7-day and 28-day compressive strengths as well as the standard deviations of the composite cementitious grouting materials prepared with different mix ratios and different dispersion methods. It is worth noting that the incorporation of large amounts of FA into the slurry significantly reduces its mechanical properties. The addition of fly ash may have an impact on cement hydration. The low activity of fly ash or coarser particle size may slow down the overall hydration reaction rate and affect the strength of concrete, especially in the early stage. A comparison of Ref and CFAS specimens revealed that the 7d and 28d compressive strengths decreased by 5.18 MPa and 0.91 MPa after replacing 20% of cement in the cementitious material with an equal amount of FA. This is as expected because the rate at which the hydration reaction of FA produces hydrated calcium silicate (hydration rate) is significantly lower than that of cement (Sun et al., 2019). At 28 days of age, the hardened FA composite cementitious grouting material has less strength as compared to Ref specimens as there is less calcium silicate hydrated in the high FA dosed CFAS specimens and the strength of the composite cementitious material is mainly provided by calcium silicate hydrated.

The inclusion of 0.023% CNTs in the FA composite cementitious grouting material led to a notable enhancement in the strength of the cured specimens. The 7-day and 28-day compressive strengths witnessed increases ranging from 2.09% to 14.95% and 24.38%–32.87%, respectively, when compared to the Ref and CFAS specimens. Studies have indicated that the expansive specific surface area of CNTs plays a pivotal role in nucleation effects, facilitating the generation of hydration products that densify the microstructure of the cement matrix (Wu et al., 2022). Furthermore, SEM images presented in Figure 5 illustrate that CNTs can establish a bridging network structure within the cement matrix, effectively filling and

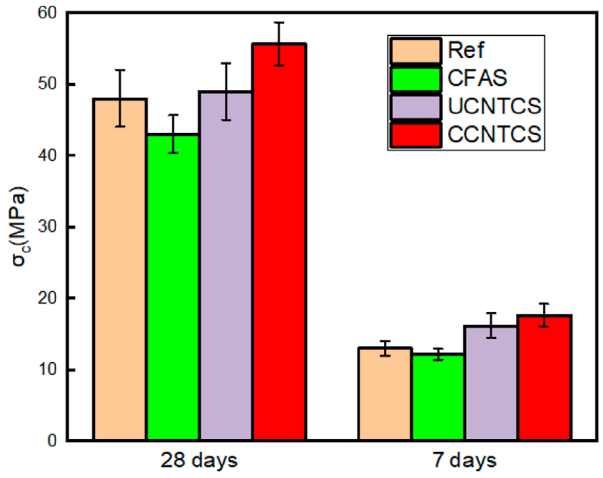

FIGURE 4
Compressive strength of four groups of specimens at 7d and 28d.

bridging microcracks and pores, thereby impeding crack formation and progression under loading conditions (Chen and Akono, 2020).

It is worth noting that according to the error bar, the 7d compressive strength of UCNTCS group is equivalent to that of CCNTCS group, while the 28d compressive strength is significantly different from that of CCNTCS group. The essence of this difference is closely related to the phased hydration characteristics of the cement-fly ash system and the time dependence of CNT dispersion stability: in the early stage (7d), cement clinkers (C_3S, C_3A) are in the rapid hydration period, and a large amount of C-S-H gel fills the matrix pores quickly (Sun et al., 2019). At this time, although the ultrasonically dispersed CNTs in the UCNTCS group have a small amount of agglomeration, their short-term nucleation effect can still promote local hydration, which offsets the early dispersion advantage of CNTs in the CCNTCS group, so the 7d strengths of the two groups are similar; in the late stage (28d), the hydration of cement clinkers enters a plateau, and strength growth mainly depends on the secondary hydration of fly ash (active SiO_2 and Al_2O_3 in FA react with residual $Ca(OH)_2$ in cement to generate C-S-H, Chen and Akono, 2020). At this time, CNTs fixed on the FA surface by covalent bonds in the CCNTCS group maintain uniform dispersion for a long time, continuously providing nucleation sites in the cement-FA interface transition zone (ITZ), accelerating secondary hydration and bridging micropores; in contrast, the ultrasonically dispersed CNTs in the UCNTCS group are prone to secondary agglomeration due to the lack of stable bonding (Kim et al., 2019), forming stress concentration zones around the agglomerates, and the CNTs damaged by ultrasound cannot effectively promote FA reaction, leading to stagnant strength growth. This situation also indicates that CNTs prepared by traditional dispersion methods had adverse changes in the subsequent curing process, which ultimately made it difficult for them to exert the strengthening effect. Finally, the compressive strength of CCNTCS group was 13.61% higher than that of UCNTCS group. The improvement of the mechanical properties is mainly due to the following three points: first, the proposed new dispersion method results in the formation of strong covalent bonds between CNTs and FA, which reduces the aggregation of CNTs in the cement paste. Secondly, the proposed dispersion method of coating CNTs on the FA surface enables more CNTs to be distributed in the ITZ between cement and FA. Previous studies have shown that CNTs at the interface help promote the hydration reaction at the ITZ, resulting in a denser ITZ of cement and FA. (Li et al., 2018). Finally, this method can reduce the damage caused by huge ultrasonic energy to the length and functional groups of CNTs in traditional ultrasonic treatment methods, so as to give full play to the bridging effect of CNTs. The 28d strength of the CCNTCS group is 13.61% higher than that of the UCNTCS group, and the core reason for this macroscopic difference is the optimization of the width and crack rate of the cement-FA interface transition zone (ITZ) by CNTs, which will be elaborated in Section 3.4.The above differences in macroscopic mechanical properties are essentially a direct reflection of the structural regulation of the cement-FA interface transition zone (ITZ) by CNTs, and the specific microscopic mechanism will be further analyzed in Section 3.4.

3.4 Description of the ITZ

Combined with the macroscopic mechanical property results in Section 3.3, it can be seen that the structural optimization of the cement-FA interface transition zone (ITZ) is the core microscopic reason for the improvement of the compressive strength of composite cement grouting materials by CNTs. Replacing cement with FA in cement grouting material can improve the workability of the material and reduce the cement content. The reduction in cement use means a reduction in the cost of the grouting project as well as in energy consumption and CO2 emissions throughout the life cycle of the project. However, FA hydrates more slowly than cement, resulting in the formation of ITZ between the two substrates. The results show that the ITZ has higher porosity and larger average diameter than the normal cement zone due to insufficient hydration (Claramunt et al., 2019). This is mainly because the reaction rate of this part of cement particles is low, and it cannot fully react to form hydrated calcium silicate (C-S-H), and the unreacted calcium hydroxide will remain in the interface transition zone, forming calcium hydroxide precipitation. As a result, there is only a small amount of C-S-H in the ITZ, but a large number of calcium hydroxide crystals. Calcium silicate hydrate is known to be the major strength contributor in cementitious materials, while calcium hydroxide has lower strength and contributes less to the strength of cementitious materials. In addition, high levels of calcium hydroxide tend to cause the cement matrix to expand, which can lead to cracking. As a result, the ITZ can become a weak point in the cement-hardened matrix, which can weaken the mechanical properties and durability of the grouting material.

In order to reveal the effect of CNTs on the ITZ of the grouted material, firstly, the rupture surface of the specimen after the mechanical test was imaged using BSE as shown in Figure 6a. Subsequently, as shown in Figures 6b–d, in order to distinguish between FA, cement particles and ITZ regions in the BSE images, the elemental distributions of Al, Si and Ca on the rupture surface were obtained using an electron probe (EPMA). Indeed, among the main components of the composite cementitious grouting material, the FA has a high percentage of aluminum (Al_2O_3 is 29.09% of FA),

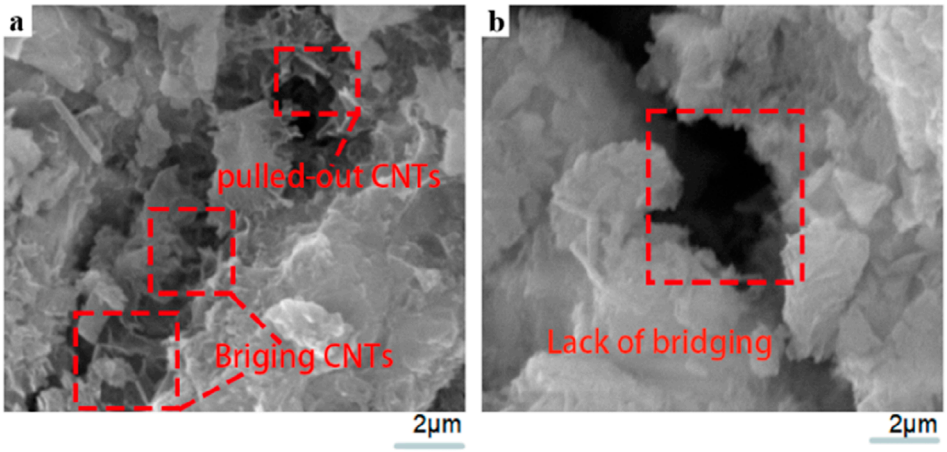

FIGURE 5
SEM images of the fracture surface of the sample in **(a)** CCNTCS and **(b)** Ref group.

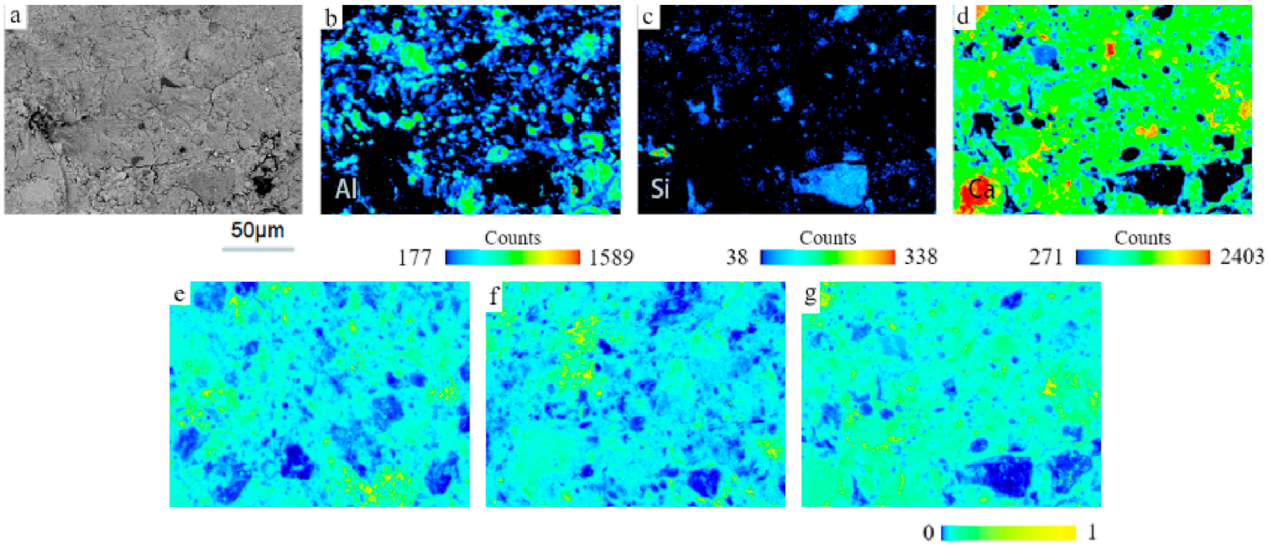

FIGURE 6
(a) Typical BSE images of fracture surfaces of FA-containing grouted materials and the distribution of corresponding elements **(b)** Al, **(c)** Si, and **(d)** Ca in the BSE images. Normalized Ca/Si ratio results for the fracture surface of **(e)** CFAS, **(f)** UCNTCS and **(g)** CCNTCS specimens after mechanical testing.

while the cement particles contain very little aluminum (Al_2O_3 is 5.71% of cement). Therefore, the distribution of aluminum elements is predominantly FA, which enables the location of FA in the BSE image to be determined, as shown in Figure 6b. However, due to the large span of FA values, it is difficult to further determine the boundary between FA and cement in Figure 6b.

Next, the Ca/Si ratios of the BSE images were calculated by a MATLAB program and the results were normalized for comparison between different samples. Previous studies have shown that the Ca/Si ratio can be used to determine the boundary between ITZ and the cement matrix because the higher concentration of Ca(OH)2 in the ITZ of cement and FA ultimately results in a higher Ca/Si ratio than in ordinary cement matrices (Chen et al., 2023). The calculated normalized Ca/Si ratios for CFAS, UCNTCS and CCNTCS samples are shown in Figures 6e–g. To quantitatively analyze the ITZ width of cement/FA and its cracking rate, a k-mean algorithm was utilized on the BSE images to identify cracks. Then, as shown in Figure 7A, the image expansion method was used to calculate the average Ca/Si ratio at different distances from the fly ash and the crack rate of the microstructure within the boundary range.

Figure 7b shows the average Ca/Si ratio at different distances from FA particles in CFAS, UCNTCS and CCNTCS samples. Since ITZ of cement/FA has a higher Ca/Si ratio than that of cement matrix, the Ca/Si ratio drop point can be used as the boundary between ITZ and cement matrix. It can be seen that the width of the ITZ of the CFAS samples is about 21 μm, whereas the addition of ultrasonicated or coated dispersed CNTs reduces the width of the ITZ to 16–17 μm, with a reduction rate as high as 19.0%–23.8%.

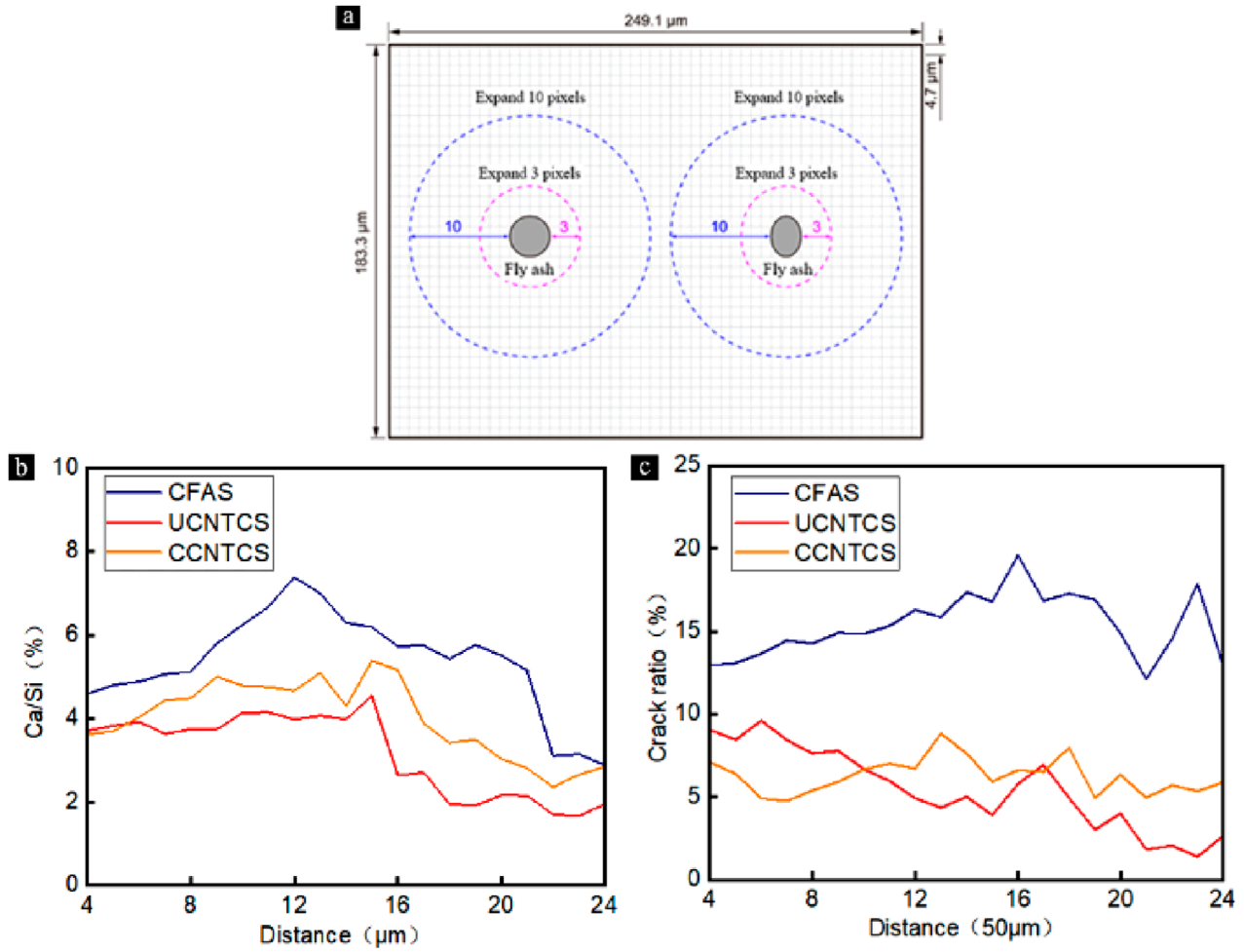

FIGURE 7
(a) Schematic diagram of image expansion method, **(b)** Average Ca/Si ratio and **(c)** crack ratio in ITZ at boundaries of different pixel units from FA particles.

In addition, the Ca/Si ratios of the UCNTCS samples were lower than those of the CFAS and CCNTCS specimens, suggesting that more hydrated calcium silicate was formed in the ITZ of the UCNTCS samples, which contributed to the improvement of the ITZ micromechanical properties.

Time-series tests (1d, 3d, 7d, 28d) further reveal the dynamic hydration evolution: at 1d, the ITZ width of the CCNTCS group is 22 μm (25 μm for the CFAS group), and CNTs have induced the formation of needle-like C-S-H; at 3d, the ITZ shrinks to 19 μm, and C-S-H interweaves into a network; at 7d, the secondary hydration of FA starts, and the ITZ width is 17 μm; at 28d, the ITZ decreases to 16 μm, and $Ca(OH)_2$ is completely consumed (TGA shows hydration degree 41.5%, higher than 36.8% of the UCNTCS group). This process explains the time-dependent difference in macroscopic strength (Sun et al., 2019; Chen et al., 2023).

More importantly, the incorporation of CNTs into the composite cement grouting material can significantly reduce the crack rate in the ITZ. After CNTs modification, the cracking rate in ITZ was significantly reduced to only 6%–8%. Comparing UCNTCS and CCNTCS samples, it can be found that the ITZ crack rate of the samples prepared by coating CNTs on the FA surface is lower, because this method can achieve better dispersion effect, and these fully dispersed CNTs can fill the microcracks in the cement matrix. However, CNTs treated with ultrasonic dispersion still showed agglomeration, and even additional micro-cracks were formed in severe cases. In addition, the huge energy in the ultrasonic treatment process will destroy the functional groups on the surface of CNTs, affecting their nucleation effect, and ultimately making it difficult to exert the enhancement effect.

3.5 Microstructure and fractal characteristics of fracture surface

Under loading, the hardened cementitious grouting material undergoes a microdestructive process from damage to fracture, ultimately forming a unique microform on the rupture surface of the material (Park et al., 2021). Previous studies have shown that the microstructure of the rupture surface of porous materials is highly correlated with the material's mechanical properties (Su et al.,

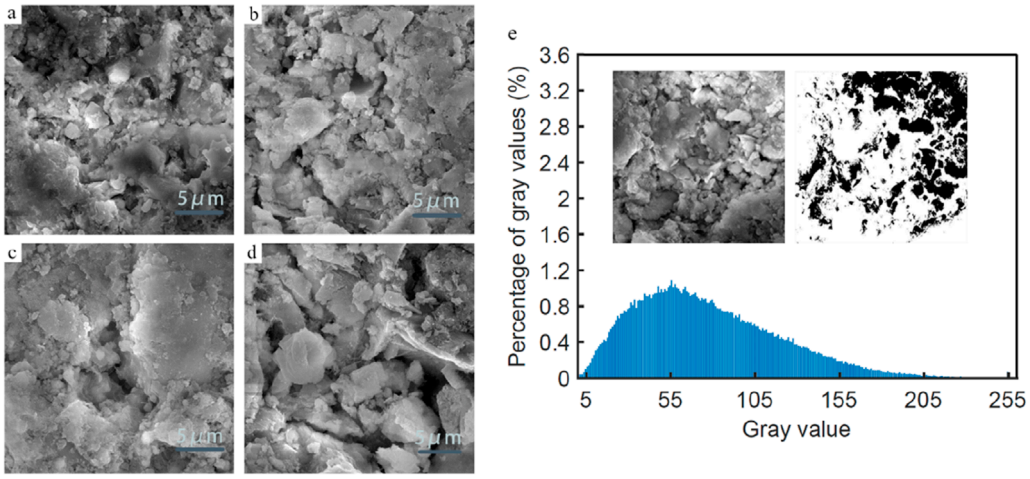

FIGURE 8
SEM images of the fracture surfaces of **(a)** Ref, **(b)** CFAS, **(Cc)** UCNTCS and **(d)** CCNTCS specimens after mechanical testing. **(e)**Relationship between gray values and pixel values of fissure surfaces in SEM images of cement matrices.

2023). Therefore, the extent of damage to the porous material can be further assessed by observing the micro-morphological characteristics of the rupture surface. In this section, SEM was used to observe the rupture surfaces of the hardened cementitious grouting materials after mechanical testing and combined with fractal theory to quantitatively characterize the extent of destruction and damage to the materials.

Figure 8 shows the SEM images of the rupture surfaces of the 4 groups of specimens. Comparing Ref and CFAS specimens reveals that replacing 20% of the cement in the cementitious grouting material with an equal amount of FA significantly increased microporosity and microcracks in the material matrix. A few unreacted round fly ash particles can be seen in Figure 8b. This is mainly due to the weak activity and gelling ability of FA, which leads to the loose microstructure of the matrix. In particular, the pores of CFAS samples were not filled with hydration products, which became a key factor in the significantly lower mechanical properties of the samples compared with the other three groups. The incorporation of CNTs significantly reduced the porosity and pore size, and needle-like hydration products appeared in the pores. It has been shown that CNTs with high specific surface area can provide nucleation sites for cement hydration. These needle-like substances are the result of hydration of cement on the surface of CNTs (MacLeod et al., 2021). In addition, the hydration products developed along CNTs, and the two ends were embedded in different parts of the hydration products, forming a unique bridge structure (Shi et al., 2019), which contributes to the improvement of the mechanical properties of hardened cementitious composites. In order to quantitatively analyze the enhancement effect of CNTs on the microstructure of cementitious grouting materials, this study further characterized the degree of destruction and damage of the materials in conjunction with fractal theory.

In the last couple of decades, fractal dimension theory has been extensively applied to the study of porosity materials. The researchers proposed that the essence of the damage of the porous materials by external loading is the superimposition of nonlinear microdeformations within them (Wang et al., 2023). Therefore, the fractal box overlay method followed in previous studies was used to calculate the specimen rupture surface fraction characterization after mechanical testing. As shown in Figure 8E, the gray threshold of the SEM image is first determined, and then the SEM image is binarized. Combined with the initial SEM image, it can be found that the white areas in the binarized image represent the complete and homogeneous parts of the original SEM image, while the black areas represent the broken and rough parts of the original SEM image. The principle and method of fractal dimension calculation are as follows:

assuming $B \in R^n$, $B \neq \emptyset$, $\forall r > 0$, $Nr(B)$ represents the smallest n-dimensional square necessary to cover the n-dimensional set B, with r denoting the side length of the square. As r approaches 0, the fractal box dimension d can be expressed as:

$$N_r(B) \propto 1/r^d \tag{1}$$

Then d is said to be the fractal dimension of the set B. At this point there exists a unique positive number a such that:

$$\lim_{r\to 0} \frac{N_r(B)}{1/r^d} = a \tag{2}$$

Taking the logarithm of both sides of (2) simultaneously, and later taking the absolute value of it, the result for the fractal dimension d is shown in (3):

$$d = \left|\lim_{r\to 0} \frac{\lg a - \lg N_r(B)}{\lg r}\right| = \left|\lim_{r\to 0} \frac{\lg N_r(B)}{\lg r}\right| \tag{3}$$

According to the above method, the fractal dimension of the rupture surface of four groups of hardened cementitious grouting materials can be calculated. The specific calculation process is shown in Figure 9a. Initially, black pixel squares with different edge lengths are chosen to encompass the binarized SEM image, and the count of squares $Nr(B)$ necessary to cover the black region is conducted. As the edge length r rises, the count of squares essential to cover the black region decreases. Following this, the fractal dimension can

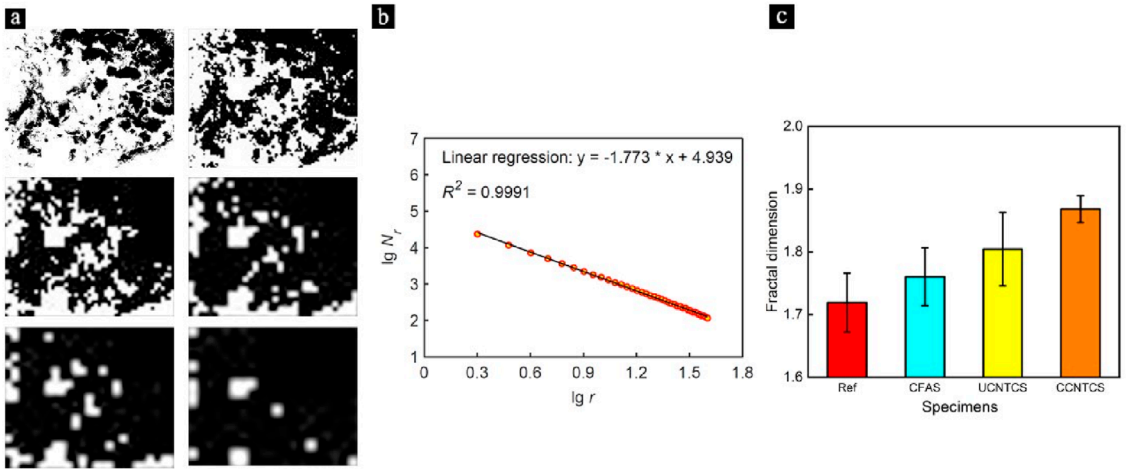

FIGURE 9
(a) fractal box covering process and **(b)** fitting of fractal dimension of binary image of fracture surface. **(c)** Fractal dimension of fracture surface for different group specimen.

be quantified by plotting the scatter diagrams of lgr and lg $Nr(B)$ mathematically, with the outcomes displayed in Figure 9b.

In order to minimize the randomness and error of the calculation results, eight specimens were randomly selected for each group, and we performed SEM scans on the fracture surfaces of the selected specimens and calculated their fractal dimensions, which are shown in Figure 9c. It is generally believed that the fractal dimension can represent the complexity and roughness of the fractal, that is, the larger the fractal dimension, the more complex and rough the fractal. In this experiment, the fractal dimension only reflects the roughness of the fracture surface of the sample, and can not directly reflect the performance of the sample. Due to the high uniformity of pure cement grouting material (Ref sample), its fracture surface is relatively smooth, and the corresponding fractal dimension is 1.72. When 20% of the cement in the grouting material is replaced with the same amount of fly ash, the fractal dimension is increased to 1.76, because the incorporation of fly ash destroys the uniformity of the cement grouting material, resulting in the reduction of the integrity of the fracture surface. The fractal dimension of ultrasonic dispersed carbon nanotubes is 1.80, and that of coated dispersed carbon nanotubes is 1.87. This is because the addition of carbon nanotubes can help the sample absorb more energy during the failure process, so the stress path inside the sample is more complicated and tortuous, resulting in more broken and rough fracture surface of the sample.

3.6 Fracture surface micro-roughness analysis

The fracture morphology method describes the rupture surface in three different scales, including shape, undulation, and roughness (Yuan et al., 2020). At the macro level, the geometry of the section is usually characterized by shape and undulation, while at the micro level, the geometry of the section is characterized by roughness. In fact, Micro-roughness refers to the degree of non-uniformity of the concave body attached to the macro-undulating surface at a smaller scale. Many scholars have studied the qualitative and quantitative evaluation methods of rock surface microroughness (Shi et al., 2021). Some scholars have proposed to assess the roughness of fracture surfaces by comparing and referring to the JRC curve of joint roughness coefficient (Barton and Choubey, 1977). On this basis, many scholars hope to achieve more accurate characterization of fracture surface roughness by developing more effective statistical induction methods and in-depth study of fractal theory (Yong et al., 2018).

The method of counting the microscopic morphology of fracture surfaces has been proposed by previous authors, which was utilized in this study to achieve the counting of the microscopic roughness of the fracture surfaces of cement grouting materials. First, the fracture surfaces formed on the specimens after mechanical testing were scanned using a VR3000 laser scanner to obtain data on the fracture surfaces. Since the fracture is not a regular circle, the matlab algorithm can be used to assist in capturing the projection of the section in the cross section direction. Next, the data from the fracture surfaces were converted into 3D point cloud data. Then, the 3D point cloud data is meshed to form a series of microscopic planes. The angle between the microscopic planes and the horizontal plane and the horizontal plane is the local inclination angle (αij). Finally, the undulation height and local tilt angle of each microscopic plane are processed by applying statistical methods to obtain the maximum value, minimum value, mean value and standard deviation. Among them, the cropping and reconstruction of the rupture surface image, the statistics of the undulation height of the rupture surface, and the calculation of the inclination angle and roughness are realized by matlab programming. A representative 3D reconstructed image of the rupture surface is shown in Figure 10.

After processing the 3D point cloud data into a grid, the matlab program is able to calculate the size of the microscopic undulation height of each grid point. The micro-height distribution of fracture surfaces for the four specimens is depicted in Figure 10a-d. Notably, the standard deviation of undulation heights

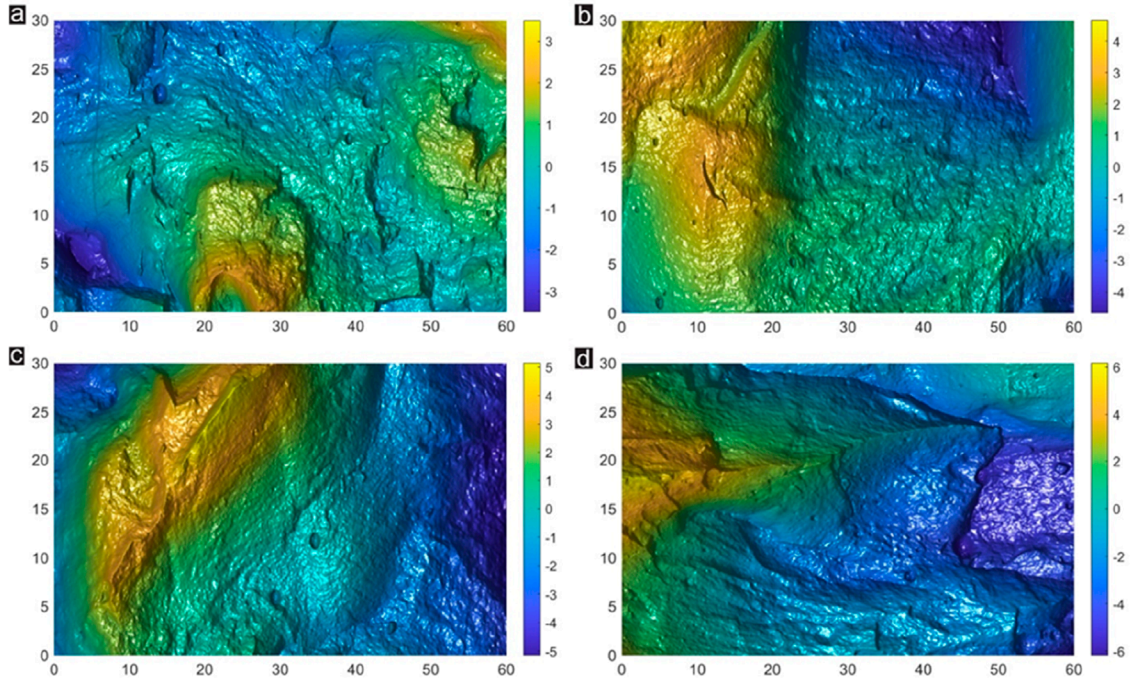

FIGURE 10
Three-dimensional reconstruction images of the fracture surfaces of **(a)** Ref, **(b)** CFAS, **(c)** UCNTCS and **(d)** CCNTCS specimens.

for the Ref, CFAS, UCNTCS, and CCNTCS groups amounts to approximately 1.08 mm, 1.78 mm, 2.31 mm, and 2.43 mm, respectively which is shown in Figure 11. This variation reveals that the CFAS group exhibits a 64.8% higher standard deviation in undulation height compared to the Ref group. This difference is attributed to the lower hydration level of FA compared to conventional cement. In CFAS group, the hydration rate of FA is slow, the hydration products are less, and the height standard deviation of fracture surface is larger, which leads to more microcracks and microvoids in the solidified matrix. Compared with ordinary cement matrix, the inherent properties of FA result in a more complex fracture surface, resulting in a curved fracture path and increased surface heterogeneity. Finally, the height standard deviation between the CFAS group and the Ref group is amplified. The nucleation effect and pore filling effect of CNTs can repair the microvoids inside the cementitious composites, and more hydration products are generated in the microvoids during the hydration process of cement with the help of CNTs, which leads to the reduction of the porosity of the hardened cement matrix. This resulted in a denser material as a whole. In addition, the CNTs bridged inside the hardened matrix were pulled out during the destruction of the specimens, and the pulling out process could help the specimens to absorb more energy, this ultimately resulted in a 114.9% rise in the standard deviation of undulation height during destruction in the UCNTCS group. In addition, the standard deviation of fracture surface fluctuation height in the CCNTCS group was 30% higher than that in the CFAS group, because CNTs coated on the FA surface not only optimized the hydration of FA and cement, but also compensated for the negative effects of adding FA on grouting materials to a certain extent. The energy absorbed by the sample in the process of failure is further increased, and the fracture surface of the sample is more broken and rough.

The calculation results of the distribution of the microscopic tilt angle of the rupture surface under uniaxial compression of different specimens are shown in Figure 12a-d. Compared with the Ref group, the distribution of local inclination Angle of specimens in CFAS group, ucncs group and ccncs group is more dispersed, indicating that the rupture surface of specimens in CFAS group, ucncs group and ccncs group has greater spatial change, and the rupture surface is relatively rough. For FA group specimens, the replacement of part of the cement by FA leads to uneven hydration reaction inside the slurry, uneven energy distribution inside the specimen, more complex crack extension paths, and rougher fracture surfaces. In UCNTCS group samples, the activation and bridging effects of CNT result in enhanced hydration and density, boosting energy absorption. This advancement allows for greater energy absorption during tensile damage, increased instantaneous energy release, and the emergence of intricate crack propagation paths, and the fracture surface roughness increases. Finally, compared to the samples in the UCNTCS group, the specimens in the CCNTCS group can absorb more energy during damage, and therefore the plane local tilt angle of the specimens in the CCNTCS group is the largest, which indicates that the surface roughness of the specimens is higher during damage.

4 Conclusion

CNTs reinforced cement provides a new way to improve the properties of cement grouting materials. However, the

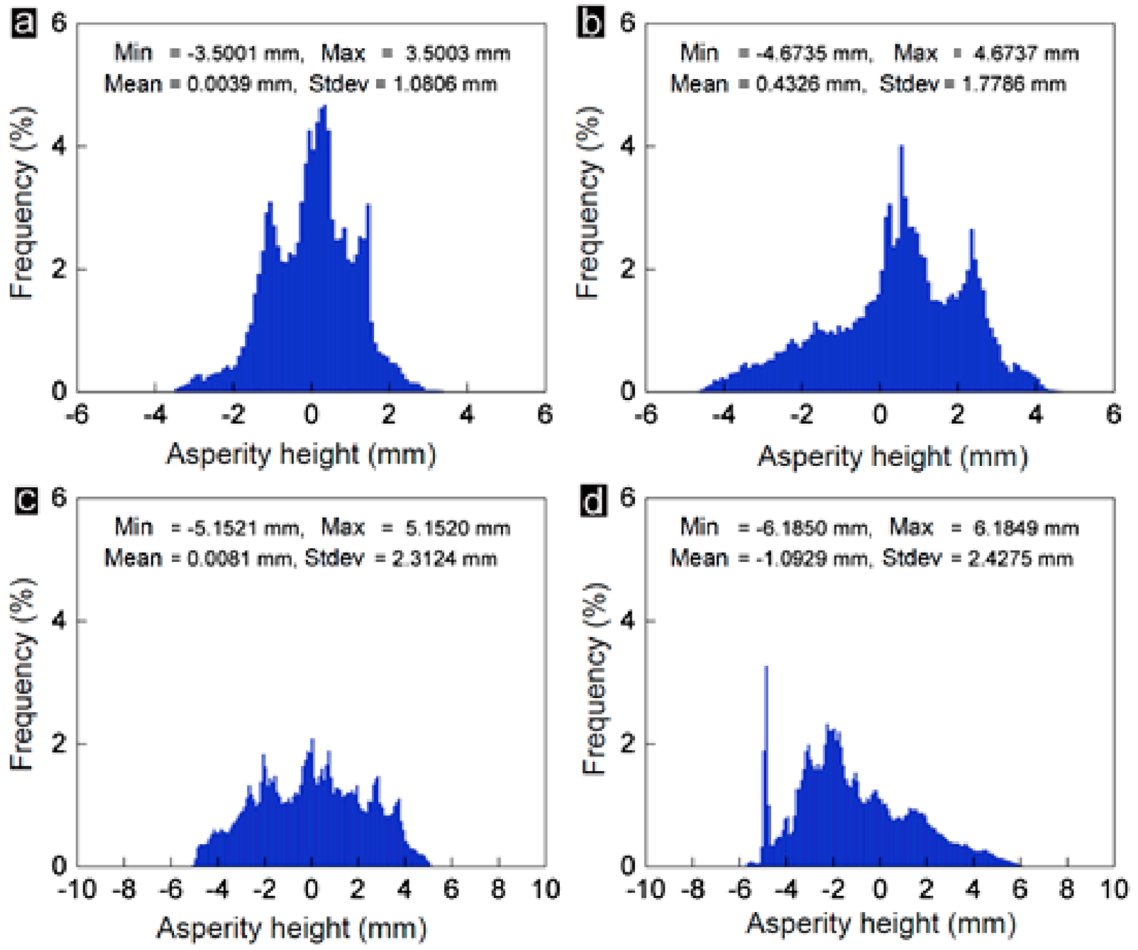

FIGURE 11
Microscopic undulation height distributions on the rupture surfaces of **(a)** Ref, **(b)** CFAS, **(c)** ucncs, and **(d)** ccncs specimens.

agglomeration of CNTs in cement slurry has seriously hindered their application in engineering. At present, the traditional dispersion method for preparing CNTs suspensions has many problems, which makes it difficult to use in engineering practice.

Therefore, in this paper, the mechanical properties and microscopic strengthening mechanism of the cementing material prepared by CNTs coated on the surface of FA were studied by combining laboratory experiments and microscopic characterization, and the following conclusions were drawn:

1. The proposed dispersion method not only achieved a good dispersion of CNTs on the FA surface, but also formed a strong covalent bond between CNTs and FA, which was conducive to preventing the separation of CNTs from the FA particle surface during hydration and reducing the number of free CNTs in the cement slurry. Free CNTs were prone to reagglomerate, which negatively affected the properties of cement. Therefore, the new dispersion method helps to promote the application of CNTs in the field of cement grouting.
2. Incorporation of carbon nanotube-coated FA into cement grouting materials can significantly improve the workability of their fresh slurries and the mechanical properties of hardened specimens. Compared with ordinary cement slurries, the replacement of 20% cement in cement-based slurries with 20.023 wt% carbon nanotube-coated FA (prepared from 0.023% CNTs and 20% FA) resulted in a significant increase of flowability by 11.6%, and an increase of compressive 14.95%–24.38%. More importantly, the enhancement rate using the encapsulated dispersion method was additionally increased by 8.89%–13.61% compared to conventional ultrasonic dispersion.
3. Addition of 0.023 wt% CNTs to FA-modified cementitious grouting materials significantly improved the cement/FA ITZs, resulting in reductions in ITZ width and cracking rate of approximately 14.5% and 50.0%, respectively. More importantly, the proposed method allowed more CNTs to be distributed at the weak ITZ and exerted their nucleation and pore-filling effects to form more and denser hydrated calcium silicate in the ITZ, which improved the micromechanical properties of the ITZ.
4. At the micro- and fine-scale, the rupture surfaces of the carbon nanotube-reinforced cementitious grouting material specimens were rougher and more broken than those of the ordinary cementitious grouting material specimens. The presence of carbon nanotubes in the carbon nanotube-reinforced cementitious grouting material repairs the

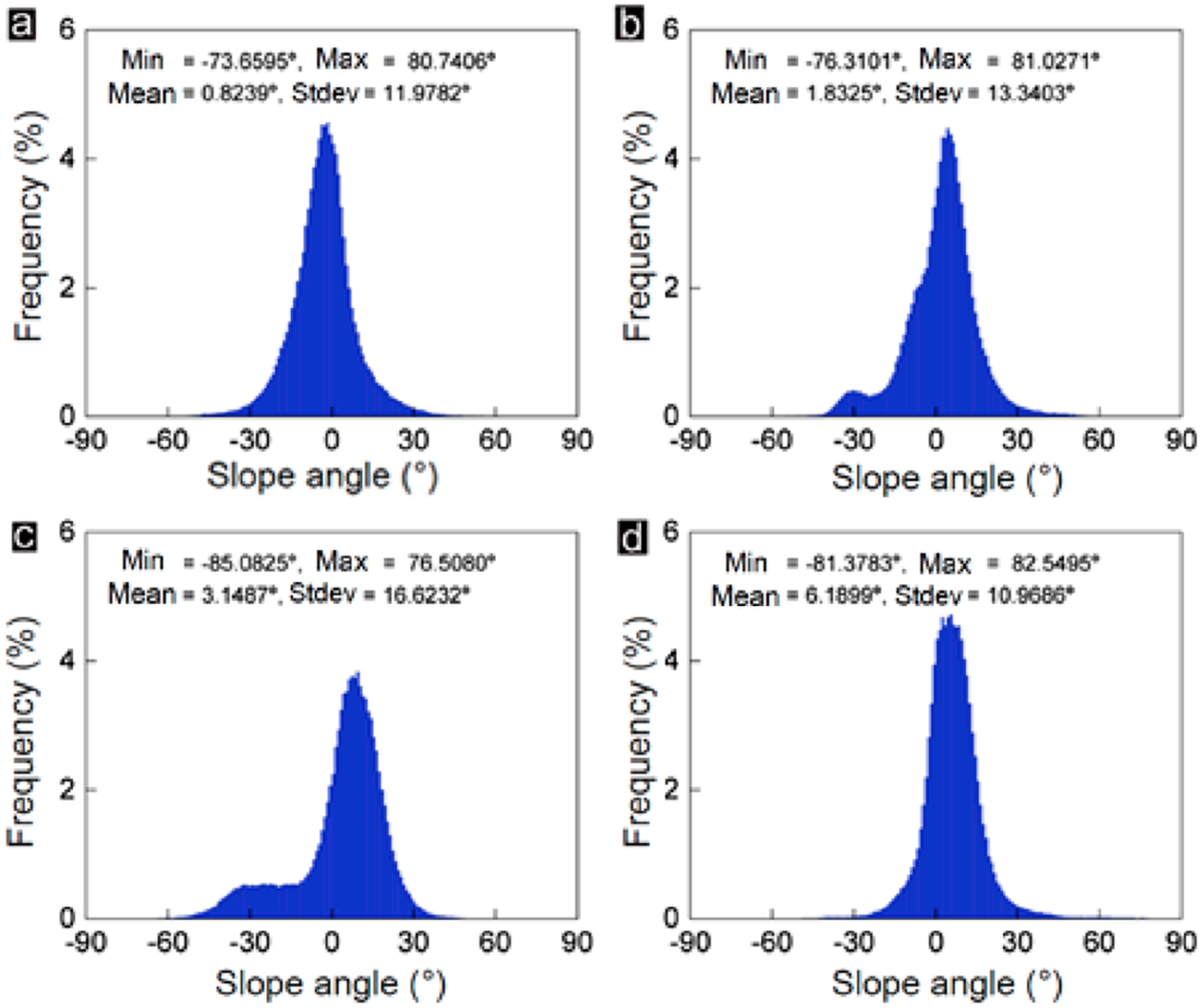

FIGURE 12
Mesoscopic slope angle distribution of the fracture surface of **(a)** Ref, **(b)** CFAS, **(c)** UCNTCS and **(d)** CCNTCS specimens.

microvoids of the specimen and improves the load resistance of the specimen, leading to a more complex and tortuous stress propagation path under loading.

From the cost-benefit perspective, the raw material cost of this technology (CCNTCS group) is about 141.1 RMB per cubic meter (cement 105.6 RMB + FA 3.3 RMB + industrial-grade CNTs 6.86 RMB + superplasticizer 25.34 RMB), which is 19.3% lower than the silica fume modified group (168.3 RMB), similar to the carbon fiber group (141.9 RMB) but with higher strength improvement (Wu et al., 2025a); the preparation energy cost is 1.02 RMB/m^3, lower than the ultrasonic dispersion group (1.17 RMB/m^3); in terms of long-term operation and maintenance, the annual operation and maintenance cost in cold-region tunnel scenarios decreases from 10 RMB/(m^3·year) to 6.67 RMB/(m^3·year), showing significant economic advantages.

CNTs will be widely used in cement grouting materials in the future. With further research into the properties and engineering applications of nanomaterials, carbon nanotubes are expected to become an important innovation driver in the field of building materials, bringing safer, durable, intelligent and environmentally friendly new materials to the construction industry, and pushing the construction industry towards a more intelligent, sustainable and efficient direction. In the future, composite coating systems of CNTs with nano-SiO_2, graphene oxide (GO) and other nanomaterials can be further developed: CNTs-nano-SiO_2 can improve impermeability through "nucleation-filling" synergy (Zhang et al., 2024), and CNTs-GO can optimize frost resistance through "barrier-bridging" synergy (Cheng et al., 2023); at the same time, it is necessary to focus on solving the long-term stability of composite coatings in harsh environments, such as interface peeling under freeze-thaw cycles (needing to adjust the coating's elastic modulus to match the matrix), expansion cracking under sulfate erosion (nano-TiO_2 can be introduced to inhibit ettringite), and nanomaterial loss under high-temperature and high-humidity conditions (needing to strengthen bonding via silane coupling agents),

so as to expand their application in deep-sea, cold-region and other projects.

Data availability statement

The original contributions presented in the study are included in the article/supplementary material, further inquiries can be directed to the corresponding author.

Author contributions

JJ: Writing – original draft, Writing – review and editing. HS: Writing – original draft, Writing – review and editing. GW: Writing – review and editing, Writing – original draft. XD: Writing – review and editing, Writing – original draft. XL: Writing – original draft, Writing – review and editing. WF: Writing – original draft, Writing – review and editing. ZL: Writing – original draft, Writing – review and editing.

Funding

The authors declare that financial support was received for the research and/or publication of this article. This work is supported by the Major Science and Technology Projects of China Coal, China (20231BY001). The funder was not involved in the study design, collection, analysis, interpretation of data, the writing of this article, or the decision to submit it for publication.

Acknowledgements

The authors gratefully appreciate this support.

Conflict of interest

Authors JJ, HS, GW, XD, XL, WF, and ZL were employed by China Coal Construction Group Limited Corporation.

Generative AI statement

The authors declare that no Generative AI was used in the creation of this manuscript.

Any alternative text (alt text) provided alongside figures in this article has been generated by Frontiers with the support of artificial intelligence and reasonable efforts have been made to ensure accuracy, including review by the authors wherever possible. If you identify any issues, please contact us.

Publisher's note

References

Abdel Rahman, R. O., Zin El Abidin, D. H. A., and Abou-Shady, H. (2013). Assessment of strontium immobilization in cement–bentonite matrices. *Chem. Eng. J.* 228, 772–780. doi:10.1016/j.cej.2013.05.034

Barton, N., and Choubey, V. (1977). The shear strength of rock joints in theory and practice. *Rock Mech.* 10, 1–54. doi:10.1007/BF01261801

Chen, J., and Akono, A. T. (2020). Influence of multi-walled carbon nanotubes on the hydration products of ordinary Portland cement paste. *Cem. Concr. Res.* 137, 106197. doi:10.1016/j.cemconres.2020.106197

Chen, S. J., Zhang, Q., Nguyen, H. D., Ren, Y., Liu, Y., Wang, W., et al. (2022). Direct 2D cement-nanoadditive deposition enabling carbon-neutral hydrogen from natural gas. *Nano Energy* 99, 107415. doi:10.1016/j.nanoen.2022.107415

Chen, W., Liu, Y., Wu, J., Lu, S., Han, G., Wei, X., et al. (2023). Enhancing cementitious grouting performance through carbon nanotube-coated fly ash incorporation. *Constr. Build. Mater.* 409, 133907. doi:10.1016/j.conbuildmat.2023.133907

Cheng, Z., Liu, Y., Wu, J., Guo, X., Chen, W., and Gao, Y. (2023). Graphene oxide-coated fly ash for high performance and low-carbon cementitious composites. *J. Mater. Res. Technol.* 25, 6710–6724. doi:10.1016/j.jmrt.2023.07.141

Chuang, W., Geng-sheng, J., Bing-liang, L., Lei, P., Ying, F., Ni, G., et al. (2017). Dispersion of carbon fibers and conductivity of carbon fiber-reinforced cement-based composites. *Ceram. Int.* 43, 15122–15132. doi:10.1016/j.ceramint.2017.08.041

Claramunt, J., Ventura, H., Toledo Filho, R. D., and Ardanuy, M. (2019). Effect of nanocelluloses on the microstructure and mechanical performance of CAC cementitious matrices. *Cem. Concr. Res.* 119, 64–76. doi:10.1016/j.cemconres.2019.02.006

Collins, F., Lambert, J., and Duan, W. H. (2012). The influences of admixtures on the dispersion, workability, and strength of carbon nanotube–OPC paste mixtures. *Cem. Concr. Compos.* 34, 201–207. doi:10.1016/j.cemconcomp.2011.09.013

Del Carmen Camacho, M., Galao, O., Baeza, F., Zornoza, E., and Garcés, P. (2014). Mechanical properties and durability of CNT cement composites. *Materials* 7, 1640–1651. doi:10.3390/ma7031640

Diamond, S. (1996). Delayed ettringite formation — processes and problems. *Cem. Concr. Compos.* 18, 205–215. doi:10.1016/0958-9465(96)00017-0

Feng, J., Yang, F., and Qian, S. (2021). Improving the bond between polypropylene fiber and cement matrix by nano calcium carbonate modification. *Constr. Build. Mater.* 269, 121249. doi:10.1016/j.conbuildmat.2020.121249

Ferrari, A. C., and Basko, D. M. (2013). Raman spectroscopy as a versatile tool for studying the properties of graphene. *Nat. Nanotech* 8, 235–246. doi:10.1038/nnano.2013.46

Ferreiro, S., Herfort, D., and Damtoft, J. S. (2017). Effect of raw clay type, fineness, water-to-cement ratio and fly ash addition on workability and strength performance of calcined clay – Limestone Portland cements. *Cem. Concr. Res.* 101, 1–12. doi:10.1016/j.cemconres.2017.08.003

Gao, Y., Jing, H. W., Chen, S. J., Du, M. R., Chen, W. Q., and Duan, W. H. (2019). Influence of ultrasonication on the dispersion and enhancing effect of graphene oxide–carbon nanotube hybrid nanoreinforcement in cementitious composite. *Compos. Part B* 164, 45–53. doi:10.1016/j.compositesb.2018.11.066

Garzón, E., Cano, M., O'Kelly, B. C., and Sánchez-Soto, P. J. (2015). Phyllite clay–cement composites having improved engineering properties and material applications. *Appl. Clay Sci.* 114, 229–233. doi:10.1016/j.clay.2015.06.006

Güllü, H., Cevik, A., Al-Ezzi, K. M. A., and Gülsan, M. E. (2019). On the rheology of using geopolymer for grouting: a comparative study with cement-based grout included fly ash and cold bonded fly ash. *Constr. Build. Mater.* 196, 594–610. doi:10.1016/j.conbuildmat.2018.11.140

Hamid Abed, M., Sabbar Abbas, I., Hamed, M., and Canakci, H. (2022). Rheological, fresh, and mechanical properties of mechanochemically activated geopolymer grout: a comparative study with conventionally activated geopolymer grout. *Constr. Build. Mater.* 322, 126338. doi:10.1016/j.conbuildmat.2022.126338

Han, G., Jing, H., Jiang, Y., Liu, R., and Wu, J. (2020). Effect of cyclic loading on the shear behaviours of both unfilled and infilled rough rock joints under constant normal stiffness conditions. *Rock Mech. Rock Eng.* 53, 31–57. doi:10.1007/s00603-019-01866-w

Jing, H., Wu, J., Yin, Q., and Wang, K. (2020). Deformation and failure characteristics of anchorage structure of surrounding rock in deep roadway. *Int. J. Min. Sci. Technol.* 30, 593–604. doi:10.1016/j.ijmst.2020.06.003

Kang, S.-T., Seo, J.-Y., and Park, S.-H. (2015). The characteristics of CNT/Cement composites with acid-treated MWCNTs. *Adv. Mater. Sci. Eng.* 2015, 1–9. doi:10.1155/2015/308725

Kaniyoor, A., and Sundara, R. (2012). A Raman spectroscopic investigation of graphite oxide derived graphene. *AIP Adv.* 2, 032183. doi:10.1063/1.4756995

Kim, G. M., Nam, I. W., Yang, B., Yoon, H. N., Lee, H. K., and Park, S. (2019). Carbon nanotube (CNT) incorporated cementitious composites for functional construction materials: the state of the art. *Compos. Struct.* 227, 111244. doi:10.1016/j.compstruct.2019.111244

Kong, X., Shi, Z., and Lu, Z. (2014). Synthesis of novel polymer nano-particles and their interaction with cement. *Constr. Build. Mater.* 68, 434–443. doi:10.1016/j.conbuildmat.2014.06.086

Langan, B. W., Weng, K., and Ward, M. A. (2002). Effect of silica fume and fly ash on heat of hydration of Portland cement. *Cem. Concr. Res.* 32, 1045–1051. doi:10.1016/S0008-8846(02)00742-1

Li, F., and Liu, J. (2018). An experimental investigation of hydration mechanism of cement with silicane. *Constr. Build. Mater.* 166, 684–693. doi:10.1016/j.conbuildmat.2018.01.164

Li, X., Li, C., Liu, Y., Chen, S. J., Wang, C. M., Sanjayan, J. G., et al. (2018). Improvement of mechanical properties by incorporating graphene oxide into cement mortar. *Mech. Adv. Mater. Struct.* 25, 1313–1322. doi:10.1080/15376494.2016.1218226

Liew, K. M., Kai, M. F., and Zhang, L. W. (2016). Carbon nanotube reinforced cementitious composites: an overview. *Compos. Part A Appl. Sci. Manuf.* 91, 301–323. doi:10.1016/j.compositesa.2016.10.020

Liu, F., Zheng, M., and Ye, Y. (2020). Formulation and properties of a newly developed powder geopolymer grouting material. *Constr. Build. Mater.* 258, 120304. doi:10.1016/j.conbuildmat.2020.120304

Liu, C., Wang, X., Chen, Y., Zhang, C., Ma, L., Deng, Z., et al. (2021). Influence of hydroxypropyl methylcellulose and silica fume on stability, rheological properties, and printability of 3D printing foam concrete. *Cem. Concr. Compos.* 122, 104158. doi:10.1016/j.cemconcomp.2021.104158

MacLeod, A. J. N., Collins, F. G., and Duan, W. (2021). Effects of carbon nanotubes on the early-age hydration kinetics of Portland cement using isothermal calorimetry. *Cem. Concr. Compos.* 119, 103994. doi:10.1016/j.cemconcomp.2021.103994

Makul, N. (2021). *Principles of cement and concrete composites*. Cham: Springer.

Mortazavi, M., Baghdadi, M., Seyed Javadi, N. H., and Torabian, A. (2019). The black beads produced by simultaneous thermal reducing and chemical bonding of graphene oxide on the surface of amino-functionalized sand particles: application for PAHs removal from contaminated waters. *J. Water Process Eng.* 31, 100798. doi:10.1016/j.jwpe.2019.100798

Nguyen, T.-H., Toumi, A., and Turatsinze, A. (2010). Mechanical properties of steel fibre reinforced and rubberised cement-based mortars. *Mater. and Des.* 31, 641–647. doi:10.1016/j.matdes.2009.05.006

Nguyen, H. D., Zhang, Q., Sagoe-Crentsil, K., and Duan, W. (2021). Graphene oxide-coated sand for improving performance of cement composites. *Cem. Concr. Compos.* 124, 104279. doi:10.1016/j.cemconcomp.2021.104279

Park, T.-H., Baek, M.-S., Hyer, H., Sohn, Y., and Lee, K.-A. (2021). Effect of direct aging on the microstructure and tensile properties of AlSi10Mg alloy manufactured by selective laser melting process. *Mater. Charact.* 176, 111113. doi:10.1016/j.matchar.2021.111113

Parveen, S., Rana, S., Fangueiro, R., and Paiva, M. C. (2015). Microstructure and mechanical properties of carbon nanotube reinforced cementitious composites developed using a novel dispersion technique. *Cem. Concr. Res.* 73, 215–227. doi:10.1016/j.cemconres.2015.03.006

Payá, J., Monzó, J., Borrachero, M. V., Peris-Mora, E., and González-López, E. (1996). Mechanical treatment of fly ashes part II: particle morphologies in ground fly ashes (GFA) and workability of GFA-cement mortars. *Cem. Concr. Res.* 26, 225–235. doi:10.1016/0008-8846(95)00212-X

Pedroso, M., and Flores-Colen, I. (2020). The influence of dimension and content of natural organic fibrous materials on the multi-performance of cement-based composites: a statistical approach. *Constr. Build. Mater.* 231, 117175. doi:10.1016/j.conbuildmat.2019.117175

Potgieter-Vermaak, S. S., Potgieter, J. H., Belleil, M., DeWeerdt, F., and Van Grieken, R. (2006). The application of Raman spectrometry to the investigation of cement: part II: a micro-Raman study of OPC, slag and fly ash. *Cem. Concr. Res.* 36, 663–670. doi:10.1016/j.cemconres.2005.09.010

Rakngan, W., Williamson, T., Ferron, R. D., Sant, G., and Juenger, M. C. G. (2018). Controlling workability in alkali-activated Class C fly ash. *Constr. Build. Mater.* 183, 226–233. doi:10.1016/j.conbuildmat.2018.06.174

Shi, T., Li, Z., Guo, J., Gong, H., and Gu, C. (2019). Research progress on CNTs/CNFs-modified cement-based composites – a review. *Constr. Build. Mater.* 202, 290–307. doi:10.1016/j.conbuildmat.2019.01.024

Shi, X., Jing, H., Chen, W., Gao, Y., and Zhao, Z. (2021). Investigation on the creep failure mechanism of sandy mudstone based on micromesoscopic mechanics. *Geofluids* 2021, 1–19. doi:10.1155/2021/5550733

Shi, H., Song, L., Zhang, H., Chen, W., Lin, H., Li, D., et al. (2022). Experimental and numerical studies on progressive debonding of grouted rock bolts. *Int. J. Min. Sci. Technol.* 32 (1), 63–74. doi:10.1016/j.ijmst.2021.10.002

Shi, H., Chen, W., Zhang, H., Song, L., Li, M., Wang, M., et al. (2023). Dynamic strength characteristics of fractured rock mass. *Eng. Fract. Mech.* 292, 109678. doi:10.1016/j.engfracmech.2023.109678

Shi, H., Chen, W., Wu, J., Rong, C., Wang, Z., Song, L., et al. (2025). Unified rock strength theory incorporating holistic consideration of macro-meso-micro defect coupling effects. *Eng. Fract. Mech.* 328, 111534. doi:10.1016/j.engfracmech.2025.111534

Song, H.-W., Pack, S.-W., Nam, S.-H., Jang, J.-C., and Saraswathy, V. (2010). Estimation of the permeability of silica fume cement concrete. *Constr. Build. Mater.* 24, 315–321. doi:10.1016/j.conbuildmat.2009.08.033

Su, Y., Zhu, J., Long, X., Zhao, L., Chen, C., and Liu, C. (2023). Statistical effects of pore features on mechanical properties and fracture behaviors of heterogeneous random porous materials by phase-field modeling. *Int. J. Solids Struct.* 264, 112098. doi:10.1016/j.ijsolstr.2022.112098

Sun, J., Shen, X., Tan, G., and Tanner, J. E. (2019). Compressive strength and hydration characteristics of high-volume fly ash concrete prepared from fly ash. *J. Therm. Anal. Calorim.* 136, 565–580. doi:10.1007/s10973-018-7578-z

Svermova, L., Sonebi, M., and Bartos, P. J. M. (2003). Influence of mix proportions on rheology of cement grouts containing limestone powder. *Cem. Concr. Compos.* 25, 737–749. doi:10.1016/S0958-9465(02)00115-4

Wang, Q., Wang, J., Lu, C. x., Liu, B. w., Zhang, K., and Li, C. z. (2015). Influence of graphene oxide additions on the microstructure and mechanical strength of cement. *New Carbon Mater.* 30, 349–356. doi:10.1016/s1872-5805(15)60194-9

Wang, D., Gao, X., Liu, X., and Zeng, G. (2021). Strength, durability and microstructure of granulated blast furnace slag-modified magnesium oxychloride cement solidified waste sludge. *J. Clean. Prod.* 292, 126072. doi:10.1016/j.jclepro.2021.126072

Wang, J., Dong, S., Pang, S. D., Zhou, C., and Han, B. (2022). Pore structure characteristics of concrete composites with surface-modified carbon nanotubes. *Cem. Concr. Compos.* 128, 104453. doi:10.1016/j.cemconcomp.2022.104453

Wang, R., Wang, G., Zhang, L., Sun, F., Cao, T., Li, B., et al. (2023). Coupled macro–*meso* damage constitutive model for fractured rocks based on logistic growth theory. *Eng. Fract. Mech.* 281, 109132. doi:10.1016/j.engfracmech.2023.109132

Wu, J., Jing, H., Gao, Y., Meng, Q., Yin, Q., and Du, Y. (2022). Effects of carbon nanotube dosage and aggregate size distribution on mechanical property and microstructure of cemented rockfill. *Cem. Concr. Compos.* 127, 104408. doi:10.1016/j.cemconcomp.2022.104408

Wu, J., Wong, H. S., Zhang, H., Yin, Q., Jing, H., and Ma, D. (2024). Improvement of cemented rockfill by premixing low-alkalinity activator and fly ash for recycling gangue and partially replacing cement. *Cem. Concr. Compos.* 145, 105345. doi:10.1016/j.cemconcomp.2023.105345

Wu, J., Yang, S., Williamson, M., Wong, H. S., Bhudia, T., Pu, H., et al. (2025a). Microscopic mechanism of cellulose nanofibers modified cemented gangue backfill materials. *Adv. Compos. Hybrid Mater.* 8 (2), 177. doi:10.1007/s42114-025-01270-9

Wu, J., Zhang, W., Wang, Y., Ju, F., Pu, H., Riabokon, E., et al. (2025b). Effect of composite alkali activator proportion on macroscopic and microscopic properties of gangue cemented rockfill: experiments and molecular dynamic modelling. *Int. J. Minerals, Metallurgy Mater.* 32 (8), 1813–1825. doi:10.1007/s12613-025-3140-8

Wu, J., Zhang, W., Shuo, Y., Jivkov, A. P., Kearsley, E., and Wong, H. S. (2025c). Polycarboxylate superplasticizer instead of ultrasonic treatment for dispersing cellulose nanofibers to strengthen cemented rockfill. *Int. J. Minerals, Metallurgy Mater.* doi:10.1007/s12613-025-3246-z

Yao, X., Shamsaei, E., Chen, S., Zhang, Q. H., De Souza, F. B., Sagoe-Crentsil, K., et al. (2019). Graphene oxide-coated poly(vinyl alcohol) fibers for enhanced fiber-reinforced cementitious composites. *Compos. Part B Eng.* 174, 107010. doi:10.1016/j.compositesb.2019.107010

Yong, R., Ye, J., Liang, Q.-F., Huang, M., and Du, S.-G. (2018). Estimation of the joint roughness coefficient (JRC) of rock joints by vector similarity measures. *Bull. Eng. Geol. Environ.* 77, 735–749. doi:10.1007/s10064-016-0947-6

Yuan, L., Zhou, F., Li, B., Gao, J., Yang, X., Cheng, J., et al. (2020). Experimental study on the effect of fracture surface morphology on plugging efficiency during temporary plugging and diverting fracturing. *J. Nat. Gas Sci. Eng.* 81, 103459. doi:10.1016/j.jngse.2020.103459

Zhang, G.-Z., Liu, C., Cheng, P.-F., Li, Z., Han, Y., and Wang, X.-Y. (2024). Enhancing the interfacial compatibility and self-healing performance of microbial mortars by nano-SiO2-modified basalt fibers. *Cem. Concr. Compos.* 152, 105650. doi:10.1016/j.cemconcomp.2024.105650